

High-field-seeking Rydberg atoms orbiting a charged wire

H. Ko and S. D. Hogan

Department of Physics and Astronomy, University College London, Gower Street, London, WC1E 6BT England, United Kingdom

(Received 19 February 2014; published 12 May 2014)

Pulsed supersonic beams of helium atoms in the high-field-seeking $52p$ Rydberg state have been guided while following helical trajectories in the electrostatic field of a charged wire suspended along the axis of a grounded cylindrical metallic tube. The operation of this electrostatic wire guide for samples in high-field-seeking Rydberg-Stark states has been investigated with dc and pulsed electric potentials applied to the wire while the guided atoms were detected by pulsed electric-field ionization. The acceptance of the guide has been determined through numerical particle trajectory simulations.

DOI: [10.1103/PhysRevA.89.053410](https://doi.org/10.1103/PhysRevA.89.053410)

PACS number(s): 37.10.De, 32.80.Rm

I. INTRODUCTION

The large electric dipole moments associated with high Rydberg states of atoms and molecules permit their translational motion to be efficiently controlled using inhomogeneous electric fields [1,2]. This has led to the experimental realization of a range of Rydberg atom and molecule optics elements for samples in both low-field-seeking Rydberg-Stark states, which exhibit positive Stark energy shifts, and in high-field-seeking states with negative Stark shifts [3–7]. However, because of (i) the greater ease with which phase-space density can be maintained during the manipulation of samples in low-field-seeking states (see, e.g., Ref. [8] and references therein) and (ii) the possibility of confining samples in these states around static electric-field minima, recent work on the development of methods for guiding [9] and electric trapping [10–14] Rydberg atoms and molecules has been directed principally toward samples in low-field-seeking states.

There are, however, several areas of research in which efficient methods for guiding and trapping Rydberg atoms and molecules in high-field-seeking Stark states are desirable. These include (i) collision and spectroscopic studies involving low angular momentum Rydberg states in which the Rydberg electron couples strongly to the ion core [15], (ii) the confinement and manipulation of antihydrogen atoms which are produced simultaneously in low- and high-field-seeking Rydberg-Stark states [16,17], and (iii) approaches to hybrid cavity-quantum electrodynamics involving atoms in high angular momentum circular Rydberg states which are always high-field seeking and exhibit quadratic Stark energy shifts [18–20]. With applications in these areas in mind, we report the results of experiments in which beams of helium (He) atoms in the triplet high-field-seeking $52p$ Rydberg state have been guided while following helical trajectories in the electrostatic field of a charged wire suspended along the axis of a grounded cylindrical metallic tube.

The geometry of this wire guide, depicted schematically in Fig. 1, is similar to those used in previously reported studies involving ground-state polar molecules in high-field-seeking states [21,22]. The guide is a cylindrical capacitor, in which an electric potential, V_c , is applied to the center wire, of radius r_w , while the outer hollow metallic cylinder, with an inner radius R_0 , is grounded. In this configuration the radial electric-field distribution, $\vec{F}_r(r)$, inside the cylinder at a position \vec{r} , where

$r = |\vec{r}|$, with respect to the center wire, is

$$\vec{F}_r(r) = \frac{V_c}{\ln(R_0/r_w)} \frac{1}{r} \hat{r}, \quad (1)$$

where \hat{r} is the unit vector in the radial direction. In this inhomogeneous electric field, atoms or molecules in high-field-seeking Rydberg-Stark states with linear Stark energy shifts, i.e., permanent effective electric dipole moments, $\vec{\mu}_{\text{eff}}$, oriented parallel to the local electric-field vector, experience a potential $U(r) = -\vec{\mu}_{\text{eff}} \cdot \vec{F}_r(r) \propto -1/r$. As a result, samples in such states can follow stable circular orbits around the center wire [23–25]. Examples of typical trajectories, that have been calculated using the parameters of the experiments reported here, are displayed in Fig. 2.

In the experiments described here, He Rydberg atoms traveled along the center wire of the guide following helical trajectories as depicted in Fig. 1(b). However, for samples with sufficiently narrow velocity distributions, it is foreseen to exploit electric-field distributions of this kind to realize electrostatic storage rings (see, e.g., Ref. [26]) in which Rydberg atoms or molecules would orbit at a fixed axial position. In addition, such a physical system, in which a particle with a permanent electric dipole moment is confined to move in a plane containing a radial electric-field distribution, is of relevance to tests of quantum mechanics in noncommutative space, via studies of angular momentum quantization [27–29].

II. EXPERIMENT

The general features of the apparatus used in the experiments reported here have been described previously [9]. Metastable He atoms traveling with a mean longitudinal speed $v_0 = 1950$ m/s in a pulsed supersonic beam were photoexcited from the long-lived 2^3S_1 state to triplet Rydberg states, with principal quantum number $n = 52$ and azimuthal quantum number $|m| = 1$. Photoexcitation was carried out using a resonant two-photon excitation scheme via the $3p$ state, which was driven by narrow-bandwidth cw laser radiation. The Rydberg photoexcitation region in the apparatus was located between a pair of metallic plates, labeled E1 and E2 in Fig. 1(a). The application of electric potentials of +0.85 V to E1 and 0 V to E2 permitted the generation of a sufficiently

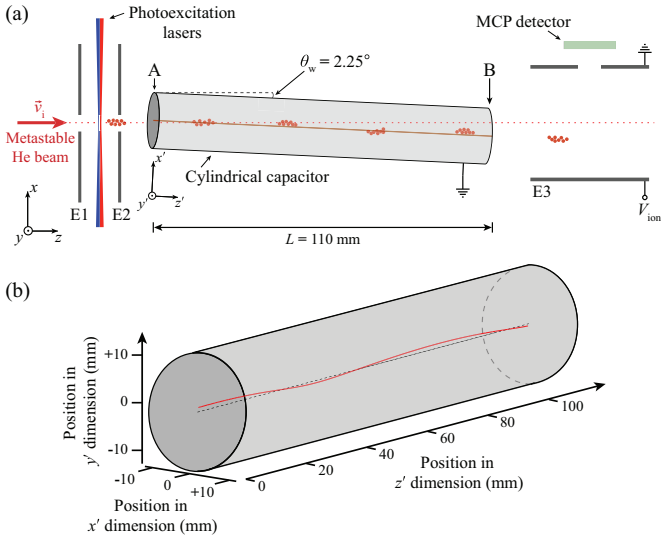


FIG. 1. (Color online) (a) Schematic diagram of the experimental apparatus (not to scale). E1 and E2 represent the metallic electrodes surrounding the Rydberg photoexcitation region, while E3 is the electrode to which a pulsed electric potential is applied to ionize the Rydberg atoms. (b) Example of a typical helical trajectory along the wire guide (solid red curve) of a He Rydberg atom in the $52p$ state.

homogeneous electric field, with a magnitude of 0.65 V/cm , at the position of photoexcitation for selective excitation of individual Rydberg-Stark states (see Fig. 3).

Following photoexcitation, the Rydberg atoms passed through a 3-mm-diameter hole in E2 and entered the part of the apparatus containing the wire guide. The guide used in the experiments was 110 mm long and was composed of a

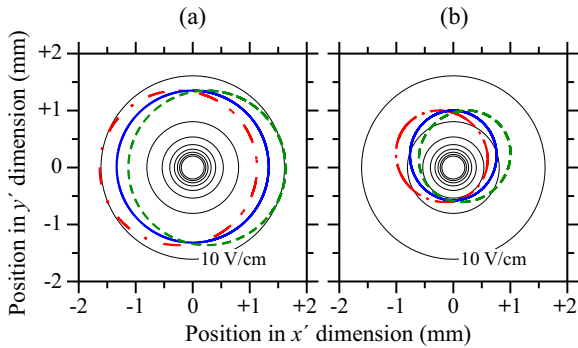


FIG. 2. (Color online) Calculated trajectories of He atoms in the $52p$ state, moving in the electric field of a cylindrical capacitor the center wire of which is suspended along the z' axis at $(x', y') = (0, 0)$. In these calculations $R_0 = 12.5 \text{ mm}$, $r_w = 25 \mu\text{m}$, and $V_c = -10 \text{ V}$. For each trajectory the initial velocity of the atoms is $\vec{v}'_i = (76, 0, 1948) \text{ m/s}$. In each panel trajectories for three initial positions are displayed. In panel (a) these are $(x', y') = (-0.25, +1.35)$, $(0, +1.35)$, and $(+0.25, +1.35) \text{ mm}$; in panel (b) these are $(x', y') = (-0.25, +1.0)$, $(0, +1.0)$, and $(+0.25, +1.0) \text{ mm}$ and in each case are indicated by the red dash-dotted, solid blue, and green dashed curves, respectively. In each panel, contours of equal electric-field strength beginning at 10 V/cm and increasing in steps of 10 V/cm are indicated by the black circles.

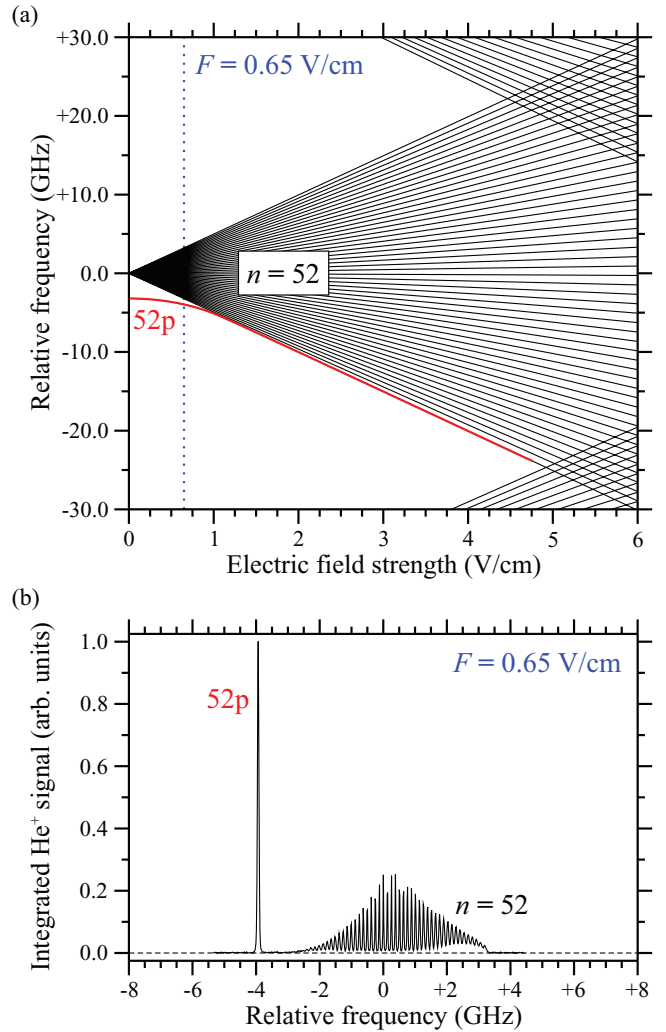


FIG. 3. (Color online) (a) Stark map of the triplet $n = 52$ Rydberg states of He for which $|m| = 1$. The $52p$ state used in the experiments is highlighted in red. (b) Experimentally measured Rydberg photoexcitation spectrum recorded in the presence of an electric field $F = 0.65 \text{ V/cm}$ [dashed vertical line in (a)].

grounded hollow cylindrical stainless-steel tube with an inside radius of $R_0 = 12.5 \text{ mm}$, along the axis of which a fine copper wire of radius $r_w = 25 \mu\text{m}$ was suspended. At the end of the guide labeled B in Fig. 1(a), the copper wire was fixed to a second perpendicular wire, of the same cross section. This wire was held tightly between two insulating screws mounted on opposite walls of the tube and separated from each other in the x dimension. At the end of the guide labeled A in Fig. 1(a), the copper wire passed through a small loop of wire that hung vertically and ensured that the center wire was positioned on the axis of the grounded tube. At this end, the center wire of the guide hung freely and was maintained under tension by the addition of a weight. Electric potentials were applied to the center wire of the guide via the loop through which it passed at the end labeled A. To ensure that this loop of wire did not impede the beam of Rydberg atoms it was located 1 mm away from the axis of propagation of the atomic beam in the x dimension [see Fig. 1(a)]. With this point fixed, the axis of the guide was rotated by an angle of $\theta_w = 2.25 \pm 0.25^\circ$

in the xz plane so that it crossed the axis of propagation of the atomic beam at a position ~ 25 mm inside the tube.

After passing through the guide the Rydberg atoms entered the detection region in the apparatus where a pulsed electric potential of $V_{\text{ion}} = +500$ V was applied to the metallic electrode labeled E3 to generate an electric field of ~ 100 V/cm which was sufficient to ionize them and accelerate the resulting He^+ ions into the positive x dimension toward a microchannel plate (MCP) detector. This detection geometry permitted the position of the Rydberg atoms in the x dimension, at the time of pulsed electric-field ionization, to be mapped onto the flight time of the He^+ ions to the MCP detector, i.e., the ion signal corresponding to atoms that were located close to (far from) the MCP detector at the time of ionization arrived at early (late) times.

III. RESULTS

To investigate the motion of samples of high-field-seeking Rydberg atoms in the inhomogeneous radial electric-field distribution surrounding the center wire of the electrostatic guide, experiments were performed with He atoms excited to the triplet, $52p$, $|m| = 1$, Rydberg state [see Fig. 3(a)]. Because of the selection rules for electric dipole transitions in the absence of external electric fields, this state cannot be populated directly by resonant two-photon excitation via the $3p$ state. Therefore a homogeneous electric field of 0.65 V/cm was generated in the Rydberg photoexcitation region to mix the $52p$ and $52d$ states. In a field of this strength, the $52p$ state attains approximately 20% of the spectral intensity of the field-free $3p \rightarrow 52d$ transition as can be seen in the experimentally recorded photoexcitation spectrum in Fig. 3(b).

The triplet $52p$ state in He has a quantum defect of $\delta_p = 0.068$ [30]. It therefore exhibits a quadratic Stark shift in weak electric fields. However, as can be seen in Fig. 3(a), when it mixes with the hydrogenic manifold of high- ℓ states, the Stark shift becomes linear in fields greater than ~ 1 V/cm. Under these conditions the effective electric dipole moment of this state is ~ 9970 D. Since a permanent effective electric dipole moment is required for the Rydberg atoms to follow stable orbits around the center wire of the guide, it was necessary to ensure that in all experiments performed the electric field experienced by the atoms was ≥ 1 V/cm. From Eq. (1), it can be determined that this is the case, for atoms within a distance of 1.5 mm from the center wire of the guide, provided $|V_c| \geq 1$ V. This condition is fulfilled in all of the experiments described below.

The $52p$ state was selected over the outermost high-field-seeking components of the manifold of high- ℓ states for two reasons.

(i) Because it is not degenerate with the high- ℓ states for which $n = 52$ in the absence of an electric field, nonadiabatic transitions to low-field-seeking Stark states in regions between the photoexcitation region and the guide, where the electric-field strength approached zero, could be avoided. This permitted flexibility in the operation of the guide in dc or pulsed modes.

(ii) For the conditions under which the experiments were performed, the spectral intensity of the transition from the $3p$

state to the $52p$ state was significantly greater than that to the outermost high-field-seeking components of the manifold of high- ℓ states, as can be seen in Fig. 3(b), leading to more efficient photoexcitation.

A. Modes of operation

The effect of the wire guide on the pulsed beams of He Rydberg atoms can be seen in the He^+ time-of-flight distributions displayed in Fig. 4(a). With the guide off, i.e., $V_c = 0$ V, the He Rydberg atoms fly directly from the photoexcitation region, along the principal axis of the experiment in the z dimension (see Fig. 1 for a definition of the coordinate system), to the detection region where they are ionized by the pulsed electric field. The resulting He^+ signal is displayed as the solid black curve in Fig. 4(a). With a constant dc electric potential of $V_c = -10$ V applied to the center wire of the guide, the maximum of the He^+ time-of-flight signal [blue dash-dotted curve in Fig. 4(a)] is shifted to later times than that recorded with the guide off and is reduced in amplitude. The shift in the flight time of the He^+ signal is attributed to a partial guiding of the ensemble of Rydberg atoms away from their initial axis of propagation and into the negative x dimension, as they

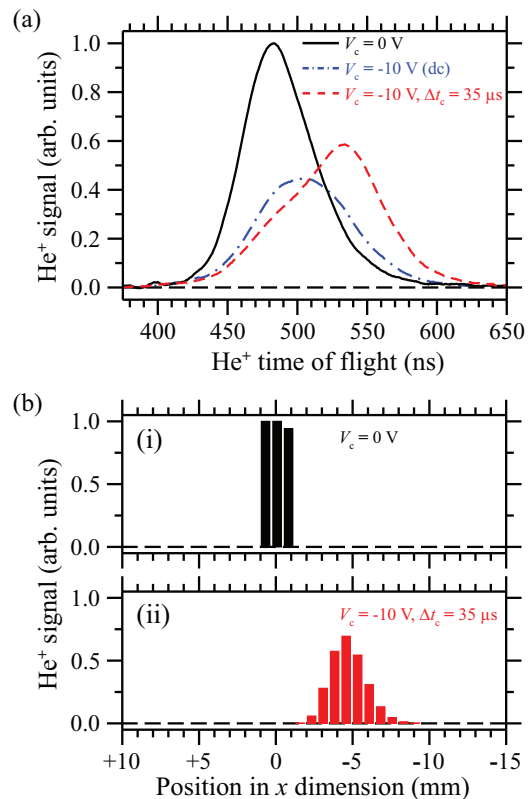


FIG. 4. (Color online) (a) He^+ time-of-flight distributions recorded with the guide off (solid black curve), a dc potential of $V_c = -10$ V applied to the guide (blue dash-dotted curve), and a pulsed potential with a duration of $\Delta t_c = 35 \mu\text{s}$ and an amplitude of $V_c = -10$ V applied to the guide (red dashed curve). (b) Calculated He atom spatial distributions at the position of pulsed electric-field ionization with (i) the guide off, and (ii) a pulsed potential with a duration of $\Delta t_c = 35 \mu\text{s}$ and an amplitude of $V_c = -10$ V applied to the guide.

orbit around the center wire of the guide. The reduction in the amplitude of the signal is a result of electric-field ionization of the atoms located closest to the wire as they travel through the guide. Under these dc operating conditions, the coupling of the Rydberg atoms into the guide is not optimal because (i) the inhomogeneous electric field between electrode E2 and the structure supporting the center wire at the beginning of the guide disturbs the phase-space distribution of the atoms as they enter the field of the guide and (ii) the atoms are coupled into the guide from a position in the negative x' dimension and positive y' dimension, with an initial velocity $\vec{v}'_i = (v_0 \sin \theta_w, 0, v_0 \cos \theta_w) = (76, 0, 1948)$ m/s, such that in the frame of reference of the guide their velocity vectors have nonzero radial components as they begin to orbit the center wire. Note that the transformation between the (x, y, z) and (x', y', z') coordinate systems associated with the atomic beam and the guide, respectively, is

$$\begin{aligned} x' &= +x \cos \theta_w + z \sin \theta_w, \\ y' &= y, \\ z' &= -x \sin \theta_w + z \cos \theta_w. \end{aligned}$$

The sets of axes associated with each of these coordinate systems are indicated in Fig. 1.

To improve the coupling of the atoms into the guide, instead of operating with dc potentials, the guide can be operated in a pulsed mode. In this way a time delay can be imposed between Rydberg photoexcitation and activation of the guide to ensure that the atoms are at the optimal position within the guide when it is activated. The optimal delay between photoexcitation and activation of the guide was determined experimentally to be $\Delta t_{\text{in}} = 20 \mu\text{s}$. Under these conditions, the center of the bunch of atoms travels a distance of ~ 39 mm in the positive z dimension before the guide is activated. At this position the center of the bunch of Rydberg atoms is located directly above the center wire of the guide in the positive y' dimension at $x' = 0$ at the activation time, and optimal coupling into the guide can be achieved. Under these conditions the atoms have zero mean radial velocity as they begin to orbit the wire. The He^+ time-of-flight signal recorded in this pulsed mode of operation with an electric potential of $V_c = -10$ V applied to the center wire of the guide for a time $\Delta t_c = 35 \mu\text{s}$ is also displayed in Fig. 4(a) (dashed red curve). In this time-of-flight distribution, the signal maximum is shifted to even later times than that recorded with the guide operated in a dc mode. The signal also has a larger amplitude because of improved coupling of the atoms into the guide and reduced ionization in the strong electric fields close to the center wire.

The experimentally measured He^+ time-of-flight distributions displayed in Fig. 4(a) correspond to a mapping of the spatial distribution of He Rydberg atoms in the x dimension in the detection region, onto a flight time of the ions to the MCP detector. The spatial distribution of atoms at this position in the apparatus can also be determined from three-dimensional numerical simulations of particle trajectories through the guide. The results of such simulations with the guide off, and with the guide operated in pulsed mode with $V_c = -10$ V and $\Delta t_c = 35 \mu\text{s}$, are presented in Figs. 4(b-i) and 4(b-ii), respectively. From these simulations, it can be seen that, with the guide operating in pulsed mode, when the atoms reach the

detection region they are displaced in the negative x dimension by ~ 5 mm with respect to their position when the guide is off. The general structure and the position of the maxima of the calculated particle spatial distributions in Fig. 4(b) agree well with the experimental time-of-flight data if, within the spatial region of interest, a displacement of 5 mm in the x dimension is mapped onto a change in He^+ flight time of 55 ns. This mapping of position to flight time has been determined from numerical calculations of He^+ trajectories in the time-dependent fields of the detection region. However, the width of the experimentally recorded time-of-flight distributions results from a combination of effects which include (i) the spatial spread of the atoms at the position of ionization, (ii) effects of blackbody transitions on the Rydberg atom dynamics in the guide and on the detection by electric-field ionization, and (iii) the temporal response of the MCP detector and associated electronics. Because of the difficulty in treating each of these effects sufficiently accurately to model the complete process of electric-field ionization and ion detection, this aspect of the experiment has not been simulated.

B. Spatial acceptance

With the guide operated in pulsed mode, the atoms can be efficiently coupled into it with close to zero mean radial velocity. The spatial acceptance of the guide for atoms with an initial velocity $\vec{v}'_i = (v_0 \sin \theta_w, 0, v_0 \cos \theta_w) = (76, 0, 1948)$ m/s can be seen in Figs. 5(a) and 5(b). In each of these figures the dash-dotted black semicircle represents the geometric constraint imposed by the hole in electrode E2 through which the atoms pass following photoexcitation and before entering the guide. In Fig. 5(a) the red shaded region represents the initial spatial positions of all Rydberg atoms that can travel along the guide without undergoing electric-field ionization when the guide is operated in pulsed mode with $\Delta t_c = 35 \mu\text{s}$ and $V_c = -10$ V. The symmetry of the guide gives rise to an equivalent spatial acceptance in the positive and negative y' dimensions. In Fig. 5(b), the blue shaded region represents the initial spatial positions of atoms that follow helical trajectories along the guide and have a final orbital radius at the end of the guide that is less than or equal to their initial orbital radius. Under the conditions of the experiments reported here this region represents the effective acceptance of the guide. From measurements of the location in the y' dimension of the photoexcitation laser beams in the experiments and comparison with numerical particle trajectory simulations it has been found that at the time when the guide is activated, when operated in pulsed mode, the center of the bunch of guided He Rydberg atoms is located at $(x', y') \simeq (0, +1.35 \text{ mm})$, at the upper edge of the shaded region in Fig. 5(b).

C. Effects of guiding time and electric potential

The result of operating the guide with pulsed electric potentials of varying duration and amplitude can be seen in Figs. 6(a) and 6(b). In each of these figures the measured signals corresponding to the He^+ time-of-flight distributions are displayed as horizontal panels. In each panel the amplitude of the ion signal is represented by the distribution of colors.

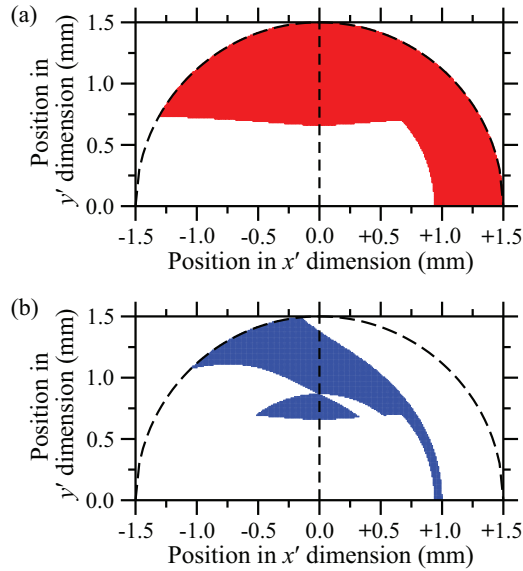


FIG. 5. (Color online) (a,b) Representations of the spatial acceptance of the guide in the x' and y' dimensions, when $V_c = -10$ V and $\Delta t_c = 35$ μ s, for He atoms in the $52p$ state with initial velocities $\vec{v}'_i = (v'_{x'}, v'_{y'}, v'_{z'})$, where $v'_{x'} = v_0 \sin \theta_w = 76$ m/s, $v'_{y'} = 0$ m/s, and $v'_{z'} = v_0 \cos \theta_w = 1948$ m/s. In each panel, the black dash-dotted curve represents the hole of radius 1.5 mm in E2 that collimates the excited Rydberg atoms before they enter the guide. The red shaded region in (a) represents the initial positions from which the Rydberg atoms can travel through the guide without undergoing electric-field ionization. The blue shaded region in (b) represents the initial particle positions from which, after a flight time of 35 μ s, the orbital radius of the guided atoms is less than or equal to their initial orbital radius.

As a point of reference, the time of flight of 485 ns associated with the peak of the He^+ signal with the guide off [bottom panel in (a) and (b)] is indicated by the dashed white vertical line in each figure.

The effect of guiding the atoms for increasing periods of time can be seen in Fig. 6(a) for a pulsed potential of

$V_c = -10$ V applied for time durations ranging from $\Delta t_c = 0$ to 45 μ s. As Δt_c is increased the He Rydberg atoms follow the center wire for longer periods of their trajectories and are therefore guided increasing distances away from their initial axis of propagation and into the negative x dimension. This can be seen via the shift in the peak of the He^+ signal to later times as Δt_c increases. In the panels at the top of Fig. 6(a), when $\Delta t_c > 35$ μ s, the guide remains activated during the time when the bunch of Rydberg atoms travels out of the grounded cylinder and through the region at the end of the guide containing the supporting wire from which the center wire is suspended. The inhomogeneous electric field in this region leads to a distortion of the bunch of guided atoms and to losses arising from electric-field ionization. These effects are reflected in the signal in the corresponding panels in Fig. 6(a).

The effect of varying the electric potential V_c has also been investigated, with the results presented in Fig. 6(b). In recording this data the guide was operated in pulsed mode and activated for a time $\Delta t_c = 35$ μ s. From these measurements it can be seen that as V_c is adjusted from 0 to -10 V the efficiency with which the atoms are coupled into the guide increases as they orbit closer to the center wire, and the flight time associated with the peak of the He^+ signal shifts to later times. The corresponding displacement of the atoms into the negative x dimension is representative of the macromotion of the detected bunch of Rydberg atoms which, because of the cw laser excitation scheme employed, has an extension in the z dimension of ~ 10 mm. If Rydberg photoexcitation was performed with a pulsed laser, generating a bunch of excited atoms with a narrow initial spatial distribution in this dimension, the micromotion of the atoms as they orbit around the center wire of the guide would become apparent as oscillations in the flight time associated with the peak of the He^+ signal as V_c is varied.

IV. DISCUSSION AND CONCLUSION

The experiments described here were performed in an apparatus operated at room temperature. As a result, depopulation

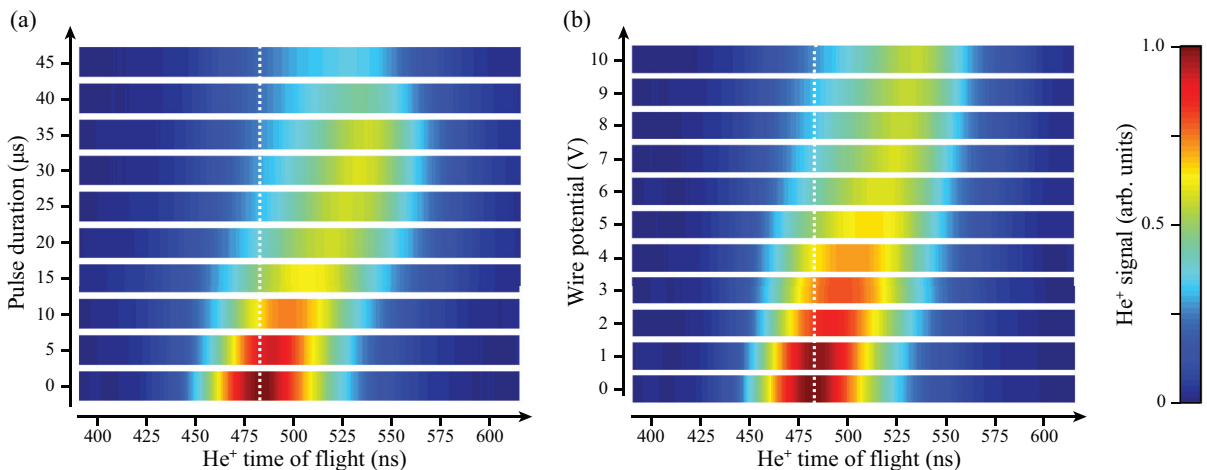


FIG. 6. (Color online) Color maps representing experimentally recorded He^+ time-of-flight distributions following pulsed electric-field ionization. The time-of-flight distributions were recorded for pulsed guide potentials with (a) pulse durations ranging from $\Delta t_c = 0$ to 45 μ s with the amplitude of the pulses held constant at $|V_c| = 10$ V and (b) pulse amplitudes ranging from $|V_c| = 0$ to 10 V with constant pulse durations of $\Delta t_c = 35$ μ s. The dashed vertical white line in each panel indicates the flight time associated with the peak of the time-of-flight distribution with the guide off. The color scale on the right is common to both (a) and (b).

of the initially prepared Rydberg state by blackbody transitions occurs at a rate which in free space is approximately $\Gamma_{\text{BB}} = (\tau_{\text{BB}})^{-1} = (130 \mu\text{s})^{-1}$ [31] and is therefore not negligible when compared to the 85- μs flight time of the Rydberg atoms through the apparatus. This blackbody depopulation rate may also be strongly modified by the electromagnetic mode structure of the environment of the guide. However, as discussed previously in the literature [12], in the presence of an electric field, blackbody transitions between Rydberg-Stark states occur predominantly between states with different values of n but approximately equal electric dipole moments. Therefore, they do not directly lead to a loss of guided atoms but instead to an increase in the range of populated states with time, and a subsequent increase in the sample's translational temperature. It will be important in future experiments to cool the apparatus to low temperatures to minimize these effects [12,32], to permit precise collision or spectroscopic studies to be performed with guided samples in selected Rydberg-Stark states.

The choice of the $|m| = 1$ Rydberg-Stark states for the experiments described ensured that the core-penetrating s state, with its large quantum defect of $\delta_s = 0.298$, did not mix with the higher- ℓ states in the presence of the electric field. This meant that the avoided crossing between the $52p$ state and the outermost low-field-seeking $n = 51$ Stark state at the Inglis-Teller limit [33] was as small as $\Delta E_{\text{IT}}/h \simeq 13$ MHz. When the atoms orbit the center wire of the guide in the experiments performed they are generally subjected to fields larger than the Inglis-Teller electric field of $F_{\text{IT}} = 4.92$ V/cm, as is evident in Fig. 2. Since a noticeable change in the guiding efficiency is not observed as V_c is increased in Fig. 6(b) to generate fields larger than F_{IT} , it is concluded that the avoided crossing at the Inglis-Teller limit and those in larger fields are traversed diabatically in the experiments. Therefore, the atoms do not lose their large electric dipole moments or evolve from the initially prepared high-field-seeking state to a low-field-seeking state as they travel along the center wire of the guide.

The rate at which the electric-field strength must increase to ensure that atoms in the $52p$ state traverse the first avoided crossing at the Inglis-Teller limit in Fig. 3(a) diabatically can be determined using a two-state Landau-Zener model [34,35]. To achieve a probability of 0.9 (0.99) for diabatic traversal of this avoided crossing, the electric-field strength must increase at a rate of 3.2 V/(cm μs) [34 V/(cm μs)]. At the time when the guide is activated, in the experiments performed in the pulsed

mode of operation, the rise time of the potential V_c is ~ 100 ns. This results in a rate of change of electric-field strength at the position of the atoms during this period of ~ 100 V/(cm μs) when $V_c = -10$ V. Therefore, in this phase of the experiments the avoided crossings at and beyond the Inglis-Teller limit are generally traversed diabatically. When the guide is active, with $V_c = -10$ V, the atoms in the center of the bunch have initial positions $(x', y') \simeq (0, +1.35)$ mm and experience electric fields ranging from 11.9 to 12.2 V/cm as they orbit [see Fig. 2(a)]. The amplitude of this effective oscillatory field is therefore ~ 0.3 V/cm, and the oscillation period lies in the range 10–100 μs . The rate at which the electric-field strength changes is therefore so low that the avoided crossings in the Stark map must be traversed adiabatically. However, the amplitude of this effective time-varying electric field is smaller than the difference in electric-field strength of ~ 0.32 V/cm between consecutive crossings in the Stark map at the corresponding field strength of ~ 12 V/cm. It is therefore concluded that as the atoms orbit the center wire of the guide they encounter few avoided crossings and therefore do not lose their large electric dipole moments. However, since blackbody transitions or collisions can lead to changes in the value of $|m|$, and hence smaller avoided crossings, it may be that these processes also contribute to ensuring that the atoms maintain a permanent effective electric dipole moment with the appropriate orientation as they travel along the guide. To disentangle these processes and study the particle dynamics in more detail, it will be necessary in the future to perform experiments in a cryogenic apparatus.

Guiding atoms prepared in high-field-seeking Rydberg-Stark states in the electrostatic field of a charged wire guide, as demonstrated here, opens up exciting possibilities for studies of the decay dynamics, collisions, and interactions of samples in such states as they are confined to orbit in miniature electrostatic storage rings. This also represents a route toward future spectroscopic studies of the couplings between the motional and internal degrees of freedom of orbiting Rydberg atoms, in a setting that may offer insights into quantum mechanics in noncommutative space.

ACKNOWLEDGMENTS

This work was supported financially by the Department of Physics and Astronomy and the Faculty of Mathematical and Physical Sciences at University College London.

-
- [1] W. H. Wing, *Phys. Rev. Lett.* **45**, 631 (1980).
 - [2] T. Breeden and H. Metcalf, *Phys. Rev. Lett.* **47**, 1726 (1981).
 - [3] D. Townsend, A. L. Goodgame, S. R. Procter, S. R. Mackenzie, and T. P. Softley, *J. Phys. B* **34**, 439 (2001).
 - [4] Y. Yamakita, S. R. Procter, A. L. Goodgame, T. P. Softley, and F. Merkt, *J. Chem. Phys.* **121**, 1419 (2004).
 - [5] E. Vliegen, H. J. Wörner, T. P. Softley, and F. Merkt, *Phys. Rev. Lett.* **92**, 033005 (2004).
 - [6] E. Vliegen and F. Merkt, *Phys. Rev. Lett.* **97**, 033002 (2006).
 - [7] E. Vliegen, P. A. Limacher, and F. Merkt, *Eur. Phys. J. D* **40**, 73 (2006).
 - [8] S. Y. T. van de Meerakker, H. L. Bethlem, N. Vanhaecke, and G. Meijer, *Chem. Rev.* **112**, 4828 (2012).
 - [9] P. Lancuba and S. D. Hogan, *Phys. Rev. A* **88**, 043427 (2013).
 - [10] S. D. Hogan and F. Merkt, *Phys. Rev. Lett.* **100**, 043001 (2008).
 - [11] S. D. Hogan, Ch. Seiler, and F. Merkt, *Phys. Rev. Lett.* **103**, 123001 (2009).
 - [12] Ch. Seiler, S. D. Hogan, H. Schmutz, J. A. Agner, and F. Merkt, *Phys. Rev. Lett.* **106**, 073003 (2011).
 - [13] S. D. Hogan, P. Allmendinger, H. Saß Mannshausen, H. Schmutz, and F. Merkt, *Phys. Rev. Lett.* **108**, 063008 (2012).

- [14] P. Allmendinger, J. A. Agner, H. Schmutz, and F. Merkt, *Phys. Rev. A* **88**, 043433 (2013).
- [15] T. P. Softley, *Int. Rev. Phys. Chem.* **23**, 1 (2004).
- [16] M. Amoretti, C. Amsler, G. Bonomi, A. Bouchta, P. Bowe, C. Carraro, C. L. Cesar, M. Charlton, M. J. T. Collier, M. Doser, V. Filippini, K. S. Fine, A. Fontana, M. C. Fujiwara, R. Funakoshi, P. Genova, J. S. Hangst, R. S. Hayano, M. H. Holzscheiter, L. V. Jørgensen *et al.*, *Nature (London)* **419**, 456 (2002).
- [17] G. Gabrielse, N. S. Bowden, P. Oxley, A. Speck, C. H. Storry, J. N. Tan, M. Wessels, D. Grzonka, W. Oelert, G. Schepers, T. Sefzick, J. Walz, H. Pittner, T. W. Hänsch, and E. A. Hessels, *Phys. Rev. Lett.* **89**, 213401 (2002).
- [18] P. Hyafil, J. Mozley, A. Perrin, J. Tailleur, G. Nogues, M. Brune, J. M. Raimond, and S. Haroche, *Phys. Rev. Lett.* **93**, 103001 (2004).
- [19] S. D. Hogan, J. A. Agner, F. Merkt, T. Thiele, S. Filipp, and A. Wallraff, *Phys. Rev. Lett.* **108**, 063004 (2012).
- [20] J. D. Carter and J. D. D. Martin, *Phys. Rev. A* **88**, 043429 (2013).
- [21] H. J. Loesch and B. Scheel, *Phys. Rev. Lett.* **85**, 2709 (2000).
- [22] M. Strebel, S. Spieler, F. Stienkemeier, and M. Mudrich, *Phys. Rev. A* **84**, 053430 (2011).
- [23] S. K. Sekatskii, *Pis'ma Zh. Éksp. Teor. Fiz.* **62**, 900 (1995) [*JETP Lett.* **62**, 916 (1995)].
- [24] S. K. Sekatskii and J. Schmiedmayer, *Europhys. Lett.* **36**, 407 (1996).
- [25] H. J. Loesch, *Chem. Phys.* **207**, 427 (1996).
- [26] J. Schmiedmayer, *Appl. Phys. B* **60**, 169 (1995).
- [27] C. Baxter, *Phys. Rev. Lett.* **74**, 514 (1995).
- [28] J.-Z. Zhang, *Phys. Rev. Lett.* **77**, 44 (1996).
- [29] J.-Z. Zhang, *Phys. Rev. Lett.* **93**, 043002 (2004).
- [30] W. C. Martin, *Phys. Rev. A* **36**, 3575 (1987).
- [31] J. W. Farley and W. H. Wing, *Phys. Rev. A* **23**, 2397 (1981).
- [32] Ch. Seiler, S. D. Hogan, and F. Merkt, *Chimia* **66**, 208 (2012).
- [33] T. F. Gallagher, *Rydberg Atoms* (Cambridge University, Cambridge, 1994).
- [34] L. D. Landau, *Phys. Z. Sowjetunion* **2**, 46 (1932).
- [35] C. Zener, *Proc. R. Soc. London A* **137**, 696 (1932).